JOURNAL OF BIOMEDICAL OPTICS 4(1), 125–136 (JANUARY 1999)

PHASE-DOMAIN PROCESSING OF OPTICAL COHERENCE TOMOGRAPHY IMAGES

K. M. Yung, S. L. Lee, and J. M. Schmitt
Hong Kong University of Science and Technology, Department of Electrical and Electronic Engineering, Clear Water Bay, Kowloon, Hong Kong

(Paper CDO-002 received December 24, 1997; revised manuscript received November 18, 1998; accepted for publication November 24, 1998.)

ABSTRACT

In optical coherence tomography (OCT), images are usually formed from the envelope of the measured interference signal. Computation of the absolute magnitude of the signal for measurement of the envelope is a nonlinear process that destroys phase information. This study explores the idea of recording and processing the phase of the OCT interference signal before calculation of the magnitudes for display. Processing the partially coherent OCT signals in the complex domain provides the opportunity to correct phase aberrations responsible for speckle noise in OCT images. We describe an OCT system that incorporates a quadrature-demodulation scheme for accurate recording of the phase and amplitude of OCT signals from single or multiple detectors. A speckle-reduction technique that works in the complex domain, called the zero-adjustment procedure (ZAP), is investigated as an example of complex-domain processing. After demonstrating its speckle-correction properties mathematically and in numerical simulations, we apply ZAP to OCT images of living skin. The results show that ZAP reduces speckle contrast in regions where scatterer density is high and expands the range of gray values in the image. However, as presently implemented, ZAP tends to blur sharp boundaries between image features. [S1083-3668(99)01501-4]

Keywords speckle; phase; zero-adjustment procedure.

1 INTRODUCTION

Optical coherence tomography (OCT) is a new medical imaging modality for imaging microscopic structures inside living tissue which is capable of producing cross-sectional images of biological tissues with a resolution of 10–15 μm to a depth of 1–2 mm.[1–7] Like medical ultrasound, synthetic aperture radar and other coherent imaging methods,[8–10] OCT is susceptible to random phase and amplitude noise that degrades image resolution and contrast.[7,11,12]

Before the future of OCT as a general-purpose tool in diagnostic medicine can be assured, the quality of the images produced by present scanners must be improved. Paradoxically, unfiltered OCT images of dense tissues usually appear sharp because the granular texture of the images gives the impression that boundaries between highly scattering tissues are demarcated even when the resolving power is poor. This phenomenon is inherent in all forms of coherent imaging and results from interference of propagating waves that combine randomly to form bright and dark regions called speckle.[13] As a source of noise, speckle is insidious because it is signal-dependent and spatially correlated and, therefore, is generally more difficult to filter or suppress than thermal noise generated by electrical devices.

Only a few studies have focused on speckle reduction in optical coherence tomography. Spatially compounding of signals from multiple detectors has been shown to reduce speckle noise, but may cause blurring across feature boundaries.[14] Although broadening the bandwidth of the source makes the speckle finer[15,16] and, therefore, facilitates speckle averaging, speckle contrast remains high as long as the sizes of scatterers or the spaces between them are smaller than the source wavelength. Filtering of speckle noise in OCT images using wavelet processing of OCT images has been attempted with some success,[17] but it cannot reverse the effects of speckle on OCT images formed by recording the magnitude of interference signals.

Since the generation of speckle is intimately connected with aberrations in the phase of the OCT signal, it is natural to ask whether processing OCT signals in the complex domain has advantages. Doppler processing of OCT signals is one application of complex-domain processing that has already been exploited to derive flow information.[18,19] The motivation behind processing of coherent (or partially coherent) signals in the complex domain is that it provides the opportunity to modify the

Address all correspondence to Joseph M. Schmitt. E-mail: eeschmit@ee.ust.hk.

1083-3668/99/$10.00

phase and/or amplitude of a signal *before* calculation of its magnitude for display.

This paper introduces basic techniques for measuring, processing, and analyzing OCT signals in the complex domain. We begin with a simple one-dimensional description of speckle formation and its effects on the complex OCT signal. Then modifications of an OCT scanner are described that permit the measurement of both the phase and amplitude of OCT signals recorded by a single detector or detector array. Using measurements obtained with the modified scanner, we investigate a particular application of complex-domain processing for speckle reduction, called the zero-adjustment procedure (ZAP), which has been applied previously in medical ultrasound.[20,21] Although still preliminary, the results illustrate the promise of coherent processing for speckle reduction and correction of local phase aberrations.

2 BACKGROUND

Before discussing specific techniques for measuring and processing complex OCT signals, let us first develop a simple one-dimensional description of the transfer function of the OCT system in the complex domain. If we assume that the tissue is made up of a large number of point scatterers, the primary variable that affects the reflectivity of the tissue is the density of scatterers. Borrowing the terminology of ultrasound, we treat the OCT image as a collection of ''*A* lines'' formed by convolution of the scatterer sequence and the point-spread function (PSF) of the OCT system. For simplicity, the analysis is restricted to the axial dimension, in which the PSF is determined by the temporal coherence function of the source.

The OCT *A*-line signal $y(x)$ results from convolution of PSF $h(x)$ with the scatterer sequence $s(x)$,

$$y(x)=h(x)\otimes s(x), \tag{1}$$

where x represents distance along the axial dimension. The PSF $h(x)$ of the light source with center wavelength λ can be specified as the product of an envelope function, represented by a sequence $g(x)$, and a complex sinusoid with a period equal to λ,

$$h(x)=g(x)e^{j2\pi x/\lambda}. \tag{2}$$

For an OCT system that employs a light-emitting diode (LED) as a light source, $g(x)$ can be approximated by a Gaussian function $e^{-4(x/l_c)^2}$ where l_c denotes the temporal coherence length of the source. In this case the source coherence length is related to the peak wavelength of emission λ_s and full width at half maximum (FWHM) bandwidth $\Delta\lambda_s$ as[22]

$$l_c=\frac{2(\ln 2)\lambda_s^2}{\pi\Delta\lambda_s}. \tag{3}$$

The wider the bandwidth of the source, the narrower the PSF. Scanning the difference between the optical paths in the reference and sample arms of the interferometer generates an *A*-line signal represented by combining Eqs. (1) and (2)

$$y(x)=[g(x)e^{j2\pi x/\lambda}]\otimes s(x). \tag{4}$$

Sampling the *A*-line $y(x)$ shown by Eq. (4) at R times per wavelength gives

$$y(n)=[g(n)e^{j2\pi n/R}]\otimes s(n) \tag{5}$$

$$=\{g(n)\otimes[s(n)e^{-j2\pi n/R}]\}e^{j2\pi n/R}, \tag{6}$$

where n is the position in the sampling sequence. To avoid aliasing, R has to be greater than 2 and, for convenience in later analyses, we set R equal to the even integer as well. From the definition of the z transform[23] of an arbitrary complex-valued signal $a(n)$,

$$Z\{a(n)\}=A(z)=\sum_{n=-\infty}^{\infty}a(n)z^{-n}. \tag{7}$$

Equation (6) can be written in the z domain as

$$Y(z)=G(ze^{-j2\pi n/R})S(z). \tag{8}$$

Now suppose $s(n)$ represents two point scatterers of amplitudes α and β that are separated by integer multiples of R,

$$s(n)=\begin{cases}\alpha, & n=0\\ \beta, & n=N_cR\\ 0, & \text{otherwise},\end{cases} \tag{9}$$

where N_cR is also an integer. For any integer N_c, the *A*-line signal, according to Eq. (6), is given by

$$y_c(n)=[\alpha g(n)+\beta g(n-N_cR)]e^{j2\pi n/R}. \tag{10}$$

In this case, constructive interference occurs and the terms $\alpha g(n)$ and $\beta g(n-N_cR)$ add. On the other hand, if the distance between the two points is increased or reduced by $R/2$, such that

$$s(n)=\begin{cases}\alpha, & n=0\\ \beta, & n=(N_d\pm\frac{1}{2})R\\ 0, & \text{otherwise},\end{cases} \tag{11}$$

where $(N_d\pm 1/2)R$ takes an integer value, the resultant signal becomes

$$y_d(n)=\{\alpha g(n)-\beta g[n-(N_d\pm\tfrac{1}{2})R]\}e^{j2\pi n/R}. \tag{12}$$

For $0\leqslant n\leqslant(N_d\pm 1/2)R$, the terms $\alpha g(n)$ and $\beta g[n-(N_d\pm 1/2)R]$ subtract instead of add as in the previous case and the backscatter signal amplitude diminishes to a very small value. Thus, the two points seem to hide each other as a result of destructive interference. In a random media such as

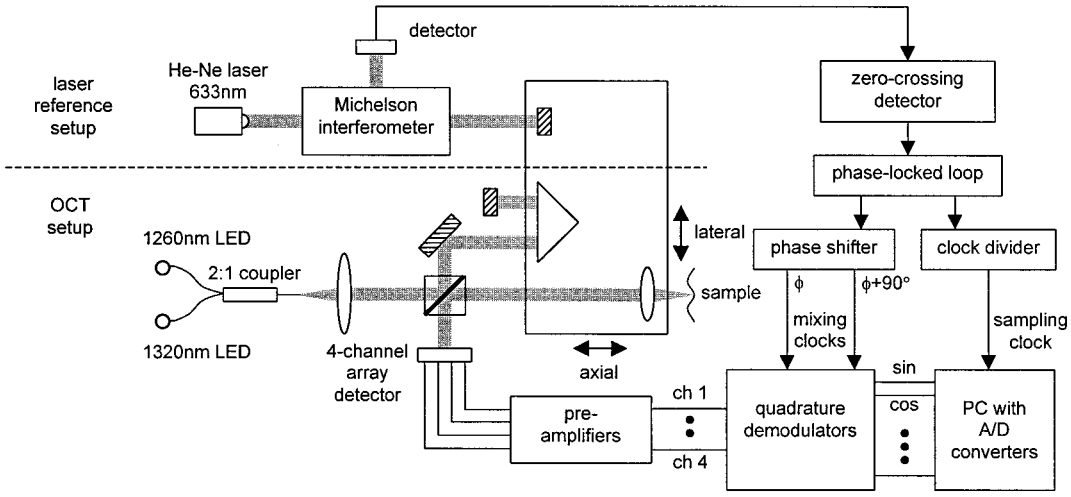

Fig. 1 Schematic of OCT scanner. The part below the broken line shows an open-air OCT system with complex signal demodulation and acquisition. The upper part is a laser reference setup for tracking the nonlinear motion of the oscillating stage (center block).

biological tissue, it is highly unlikely that all scatterers that lie along a given A line would be spaced exactly by some multiple of the center wavelength of the source so that their backscatter signals add constructively. In general, the backscatter signals would interfere constructively at some places on the line and show the distribution of scatterers correctly, while at other places they would interfere destructively and cause severe distortion of the signal envelope.

After demodulation to the baseband (i.e., removal of the carrier at the peak Doppler frequency set by the scanning velocity), Eqs. (10) and (12) become

$$y_c^{\text{demod}}(n) = \alpha g(n) + \beta g(n - N_c R), \qquad (13)$$

and

$$y_d^{\text{demod}}(n) = \alpha g(n) - \beta g[n - (N_d \pm \tfrac{1}{2})R]. \qquad (14)$$

Consider the behavior of the phases of these two signals. If the signals are treated as a sequence of complex numbers the instantaneous phase of the sequence corresponds to the angle between the abscissa and a line drawn from the origin to the location of each number plotted in the complex plane. The phase angle is bounded between $[-\pi, \pi)$. The change of phase angle at a given point in the sequence can be obtained by differentiating the continuous curve formed from the sequence of unwrapped phases.

From Eq. (13), we see that since α and β are positive real numbers and the envelope of PSF $g(n)$ is always a positive real function, $y_c^{\text{demod}}(n)$ has a constant phase equal to 0, i.e., there is no phase change along the A line. In contrast, with the same constraints on α, β, and $g(n)$ as before, plus the additional condition that α and β have comparable magnitudes, $y_d^{\text{demod}}(n)$ decreases from positive to negative when n changes from 0 to $(N_d \pm 1/2)R$. We conclude that when the demodulated signal suffers from destructive interference, the phase angle changes abruptly from 0 to $-\pi$ at where $y_d^{\text{demod}}(n)$ crosses zero. Section 3.2 introduces a method that takes advantage of the speckle-detection property of the phase of the OCT signal.

3 METHODS

3.1 OCT IMAGE ACQUISITION

Figure 1 is a schematic diagram of our OCT scanner system. Its configuration is similar to that described in an earlier article,[16] except hardware has been added for accurate measurement of both the phase and amplitude of the OCT signal. The part below the broken line shows a Michelson open-air interferometer. The two LED sources have center wavelengths of 1260 and 1320 nm, with FWHM bandwidths equal to approximately 40 nm. The light emitted by the two sources couples into the same single-mode fiber to produce a combined source with a coherence length of about 10 μm. Four detectors are used in the system, each of which receives light from a different angle from the sample volume. This detector configuration permits angular compounding for suppression of speckle.[14]

The interference signals from the four detectors are modulated at the Doppler frequency set by the axial scanning velocity. We obtain the phase and magnitude of the backscattered OCT signal by quadrature demodulation of the preamplified signals using analog circuits. Demodulation of the OCT signals before processing reduces the required sampling rate without degrading the information content of the signals. The complex-domain algorithms investigated in this study work equally well when applied to either the modulated carrier or demodulated OCT signals.

Although the translation stage is designed to execute a ramp motion in the axial direction under feedback control, its speed does not remain constant throughout the scan. If the Doppler-shifted interference signal were mixed with a constant-frequency clock, the speed variations of the stage would cause systematic errors in the measurement of the instantaneous phase of the demodulated signal. To overcome this problem, we employ a He–Ne laser reference to track the motion of the stage. The sine and cosine reference signals needed for quadrature demodulation are derived from the same laser reference clock (Figure 1). The zero-crossing detector is a comparator circuit that generates a digital high signal whenever the laser reference detector output voltage is above zero. The frequency of the square-wave signal produced by the zero-crossing detector is multiplied by four in a phase-locked loop such that there are four cycles of square wave per period of laser reference output. The square wave then passes through two D flip-flops: one triggered by rising edges and another by falling edges. Outputs from the flip-flops, like the sine-and-cosine pair, have a phase difference of $\pi/2$ while their frequency is twice that of the laser reference. This setup ensures that the mixing frequency for demodulation tracks the Doppler frequency. The sampling clock is also derived from the same laser reference to reduce the axial distortion of the images caused by the variations in the speed of the stage.

3.2 ZERO-ADJUSTMENT PROCEDURE

The zero-adjustment procedure[21] is a speckle correction method that can be applied locally to a segment of a complex signal. The signal is broken down into overlapping windows in which speckle detection is carried out independently. The speckle detection process involves locating the zeros that lie close to the spatial angular carrier (a.c.) frequency of the signal. For an a.c. sequence of spatial frequency f and wavelength $1/f=R$, its spatial angular carrier frequency is $2\pi f=2\pi/R$. Those zeros (called ''ZAP zeros,'' z_{ZAP}) that appear inside the sector in the complex plane bounded by the angular carrier frequency plus or minus a threshold angle are assumed to cause speckles. The speckle-degraded A-line signals are corrected by rotating the ZAP zeros in the complex domain. After a ZAP zero is found, it is rotated away from the signal angular carrier frequency by one fourth of the signal bandwidth.

To understand how ZAP works, consider a speckle-corrupted A line represented by

$$y_{\mathrm{SPK}}(n)=\{\alpha g(n)-\beta g[n-(N\pm\tfrac{1}{2})R]\}e^{j2\pi n/R}, \tag{15}$$

as in Eq. (12) of Sec. 2. The signal suffers from destructive interference because the two scatterers α and β are separated by $(N\pm1/2)R$. For this signal, the ZAP zero is located at $z_{\mathrm{ZAP}}=(\beta/\alpha)^{1/d}e^{j2\pi/R}$. After rotating the ZAP zero by δ rad away from the carrier frequency, we obtain the corrected A line:

$$y_{\mathrm{ZAP}}(n)=\left\{\alpha g(n)+\alpha(1-e^{j\delta})\sum_{k=1}^{(N\pm1/2)R-1}g(n-k)+[\alpha(1-e^{j\delta})-\beta]g[n-(N\pm\tfrac{1}{2})R]\right\}e^{j2n\pi/R}. \tag{16}$$

Comparing Eqs. (15) and (16), we see that ZAP adds a series of complex numbers with the same amplitude $\alpha(1-e^{j\delta})$ in the space between the two original scatterers. Thus, the magnitudes of the corrected signal in the speckled region are increased according to the magnitude of δ. The appendix presents a more detailed analysis of ZAP for the two-particle case.

To implement ZAP in this study, we first applied overlapping Hanning windows with a width close to the axial width of the system PSF to the demodulated OCT A-line signals. Each windowed complex A line was z transformed and its zeros were found by solving for the roots of a polynomial with coefficients determined by the local amplitudes and phases of the A line. The threshold value was specified in terms of the signal bandwidth. In this study, the optimum values for the threshold and rotation angles were found by trial and error to be about one fourth and one fifth of the angular bandwidth, respectively. The ZAP-corrected signal was then formed by constructing a new polynomial with roots given by the corrected zeros. Summing the magnitude of the windowed ZAP-corrected signals centered on their original locations yielded the ZAP-corrected A line. The magnitudes instead of the complex amplitudes of windowed signals were added to avoid cancellations of the ZAP-corrected signals between adjacent windows.

Ideally, more rotation is needed for signals that suffer greater loss in magnitude from speckle while less rotation is needed for signals that suffer less. However, we get no clues about the severity of the speckle from the instantaneous magnitude of the A-line signal alone. To optimize the rotation and threshold values, we relied on statistical variation of real and simulated OCT signals and on the appearance of the corrected magnitude images. We estimated the optimum rotation by finding the median value of rotations which yields the best fit to the ideal envelope in simulated A lines at different levels of recognizable speckles. The rotation used in this study (one fourth of signal bandwidth) corresponds to the case in which the mean spacing between pairs of scatterers is 2.5–3.5 times the source wavelengths.

In our four-channel system, we carried out ZAP on the complex signals from all four detectors inde-

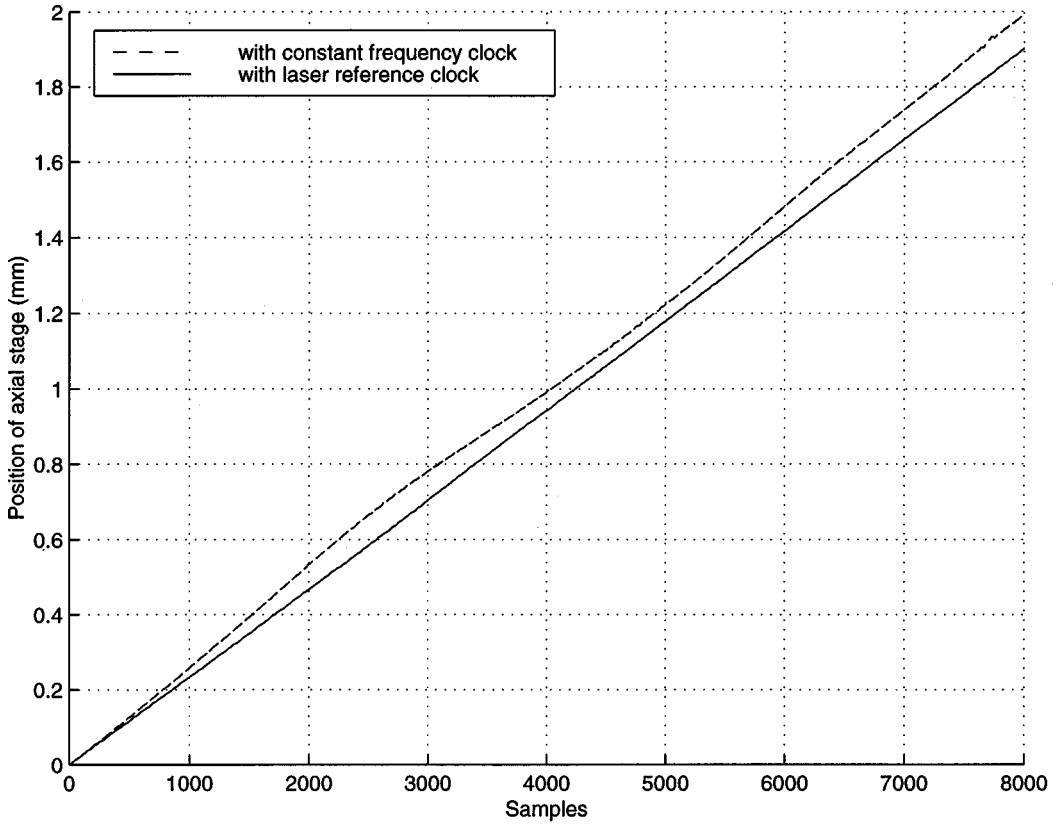

Fig. 2 Displacement of axial stage during a scanning motion sampled by a fixed-frequency clock (broken line) and the laser reference clock (solid line). The stage moves approximately 0.24 μm/sample.

pendently. The OCT images after ZAP were averaged to get the resultant image.

4 RESULTS

4.1 TEST OF THE OCT SETUP

Figure 2 shows results of a preliminary test of the tracking accuracy of the laser reference. The broken-line curve indicates the position of the stage measured by sampling the output voltage of an inductive displacement transducer built into the stage at a constant rate. Because of variations in the speed of the stage, the curve appears wavy. In contrast, the solid-line displacement curve that was measured by synchronous sampling at a rate set by the laser reference clock is straight, which demonstrates the ability of the laser reference to compensate for the speed variations.

To test the ability of the system to measure instantaneous frequency of OCT signals, we pressed several microscope cover slips coated with glycerol together to form a layered specimen with several well-defined reflections along a single *A* line. The power-spectral densities of the demodulated signals generated by reflection from the boundaries of different glass plates are shown in Figure 3. The plots in column (a) are the power-spectral densities of the *A*-line signals demodulated by mixing with a constant-frequency clock and column (b) shows the corresponding power-spectral densities of the signals demodulated by mixing with the laser clock. Observe that, unlike the spectra in column (b), the mean frequencies of the spectra in column (a) do not remain centered on zero at different depths. These data demonstrate that the system can measure the frequency content of short segments of the OCT signal in spite of the variations in the speed of the stage. Although the shape of the ensemble-averaged power-spectral density for a stationary target is determined solely by the optical spectrum of the LED source, the power spectrum of a given sample in an ensemble can be affected by rapid phase fluctuations. The power-spectral-density curve in the last row of column (b) shows such an effect.

4.2 PHASE PLOT OF OCT *A* LINE

Figure 4 shows the magnitude of an OCT *A*-line signal acquired from living skin tissue and its corresponding phase and amplitude. The magnitude (given in A/D units) was calculated as the sum of the squares of the sine and cosine components of the preamplified signal from a single detector element. The unwrapped phase curve in Figure 4(c) was differentiated numerically to obtain the local phase values in Figure 4(d). Notice the large spike-shaped phase changes that occur at around samples 200 and 400, as well as other places in the plot of

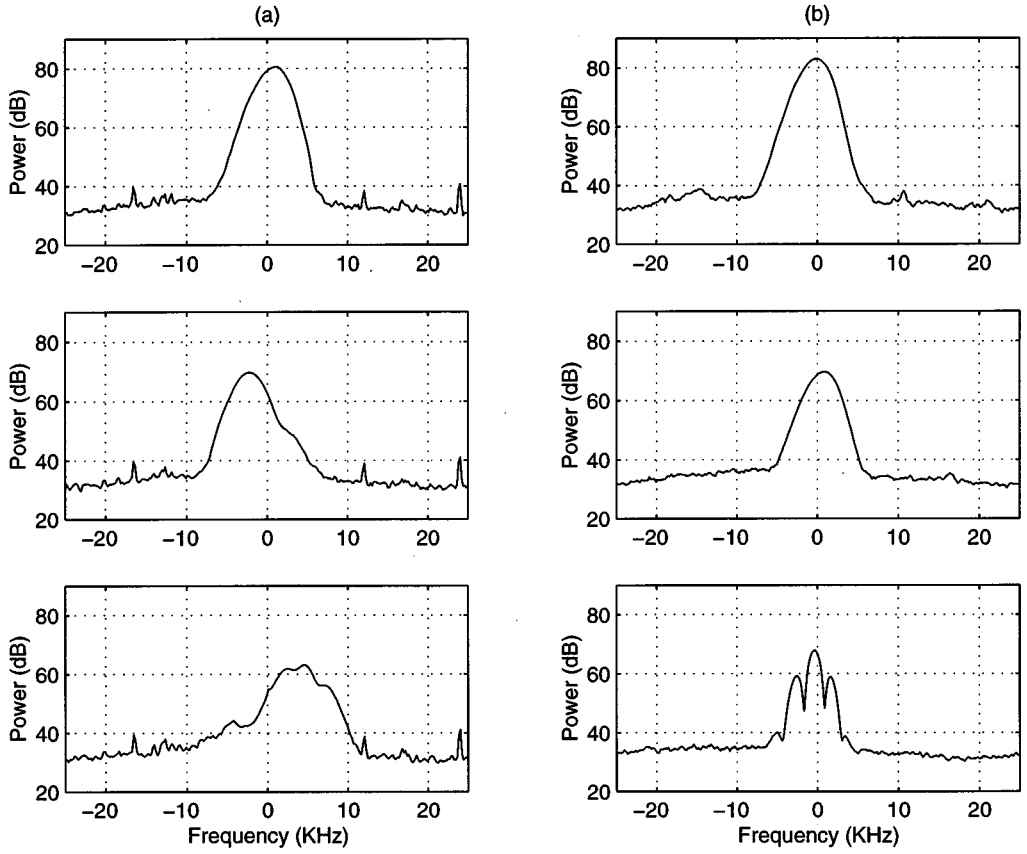

Fig. 3 Power-spectral densities of the OCT signals generated by three reflections from a stack of glass plates. The spectra of signals from different depths along the *A* line were demodulated and sampled by (a) a fixed-frequency clock and (b) the laser reference clock. Each spectrum was computed from a segment of the *A* line with a length corresponding to a free-space propagation distance of 0.2 mm. The power-spectral densities shown in the figure were calculated as an average of 100 measurements.

local phase. Such rapid phase changes are ubiquitous in signals extracted from OCT images of dense tissue. They appear to occur more frequently in heavily speckled areas of the magnitude image. However, they also occur in regions in which the signal magnitude is low and electronic noise dominates. Based on the analysis in Sec. 2, we expect the phase to change abruptly whenever destructive interference occurs. The zero-adjustment procedure, for which results are presented in the next section, is designed to correct the distortions in the envelope caused by this interference.

4.3 ZERO-ADJUSTMENT PROCEDURE

4.3.1 Simulations

Consider the short segment of a simulated *A*-line signal in Figure 5(a) which results from convolving a Gaussian PSF ($l_c = 20$ in relative units) with two scatterers separated by a distance chosen to cause severe destructive interference. Figure 6(a) is a plot of the zeros of the resultant backscatter signal in the the complex plane (the horizontal axis as the real part and vertical axis as the imaginary part). The speckle detection process begins with a search for zeros close to the angular frequency of the backscatter signal. In this example, the backscatter signal has a period of 10, which corresponds to an angular frequency of $2\pi/10 = \pi/5$. A solid tilted line at an angle of $\pi/5$ has been drawn in Figure 6(a) where a zero is located. This zero, which indicates the presence of speckle, is the so-called ZAP zero. To correct the destructive interference occurring in the backscatter signal, the ZAP zero is rotated away from the signal angular frequency by a quarter of the angular bandwidth of the signal [Figure 6(b)]. After rotation, the ZAP zero has moved to a position on the broken line which has an angle of a quarter bandwidth with respect to the solid line. A new polynomial in the z domain is formed from the corrected zeros and the corrected backscatter signal shown in Figure 5(b) is obtained by inverse z transforming the new polynomial. In this simple example, the new backscatter signal is clearly a much closer approximation of the envelope of the ideal *A*-line signal.

A more realistic simulation of ZAP for a sequence of closely spaced scatterers is shown in Figure 7. In this simulation, scatterers with random amplitudes and separations were generated by computer. The backscatter signal shown in Figure 7(b) was formed

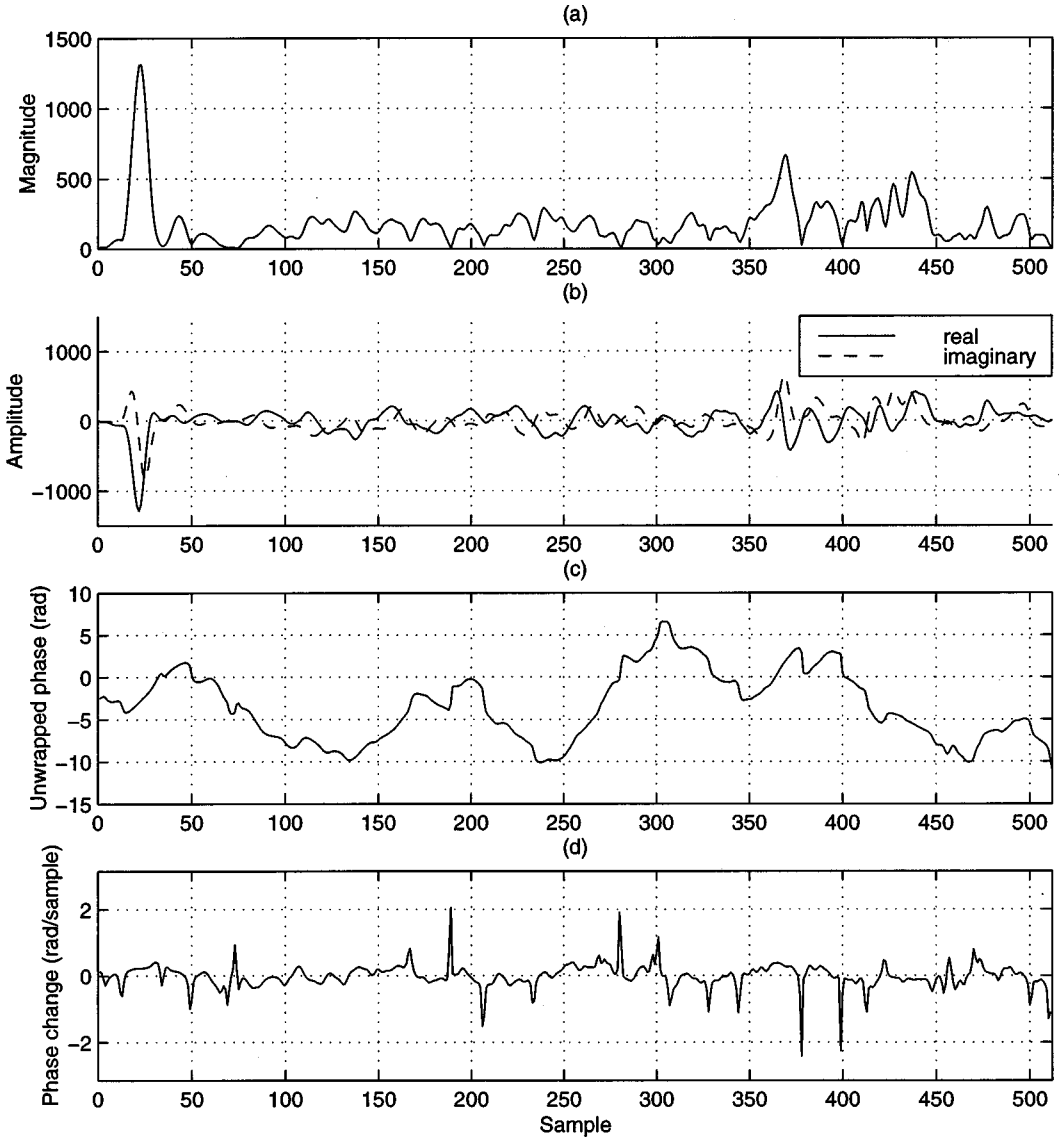

Fig. 4 Magnitude and phase of an *A*-line OCT signal acquired from living skin. The abscissa represents depth into the skin. The large peak centered on the 22nd sample is the reflection from the skin surface. The distance of penetration into the tissue was about 0.8 μm/sample. The graphs from top to bottom show (a) magnitude of the complex signal, (b) complex demodulated signal, (c) unwrapped phase of the *A* line, and (d) first derivative of the unwrapped phase.

by convolving the scatterers with the same complex PSF used in the previous simulation. The curve depicted in Figure 7(c) is the ZAP-corrected backscatter signal envelope. A comparison of Figures 7(a) and 7(c) reveals that the overall shape of the corrected envelope matches the shape of the ideal envelope much more closely than the original.

4.3.2 OCT Images

Figure 8(a) shows an image of living skin (back of the middle segment of the fifth finger) obtained with our OCT system using the laser reference setup. The image was formed by adding the magnitudes of the demodulated signals from the four detectors. After applying ZAP to each of the four channels and adding the resultant magnitudes, we obtained the result shown in Figure 8(b). A weak low-pass filter was applied in the lateral direction to all images to interpolate between *A* lines. The ZAP-corrected image appears much smoother and less grainy. ZAP reduced speckle contrast best in regions with high scatterer density and expanded the overall range of gray values in the image. However, some blurring across sharp boundaries of features in the image is evident (see, for example, the boundary of the rod-shaped structure in the center of the image, which is believed to be part of a hair follicle).

Figure 9 compares an *A* line from an image of a channel before and after application of ZAP. This *A* line is the same as that shown in Figure 4. From the previous discussion (Sec. 4.2), speckles are postulated to occur around samples 200 and 400. We can see by comparing Figures 9(a) and 9(c) that ZAP

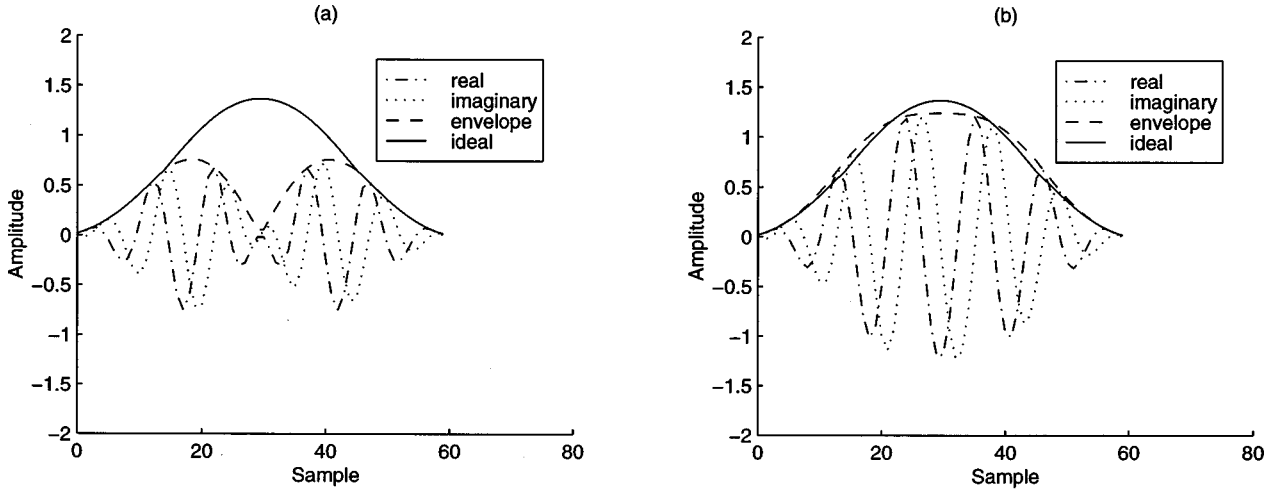

Fig. 5 Simulated backscattered signals formed from convolution of a complex PSF and two destructively interfering scatterers (a) before and (b) after ZAP.

modified the envelope of the *A*-line signal in these two regions to fill in the gaps.

To quantify the reduction of speckle contrast achieved by applying ZAP, we calculated the signal-to-noise ratio (SNR) and contrast-to-noise ratio (CNR) of the images. These quantities have been used extensively in medical ultrasound to evaluate the severity of speckle noise. The SNR is defined as

$$\mathrm{SNR}=\frac{\mu}{\sigma}, \tag{17}$$

where μ and σ are the global mean and standard deviation, respectively, of the magnitudes of the signals from which the image is formed. As in earlier studies,[17] the CNR is defined here as

$$\mathrm{CNR}=\frac{\mu_t-\mu_{\mathrm{ref}}}{\sqrt{\sigma_t^2+\sigma_{\mathrm{ref}}^2}}, \tag{18}$$

where μ_t and μ_{ref} are local means of the signals within designated target and reference windows, respectively, while σ_t and σ_{ref} are the corresponding standard deviations. Proportional to the ratio of the signal and noise powers, the SNR quantifies speckle contrast. The CNR is a measure of the available contrast between two features in an image. The

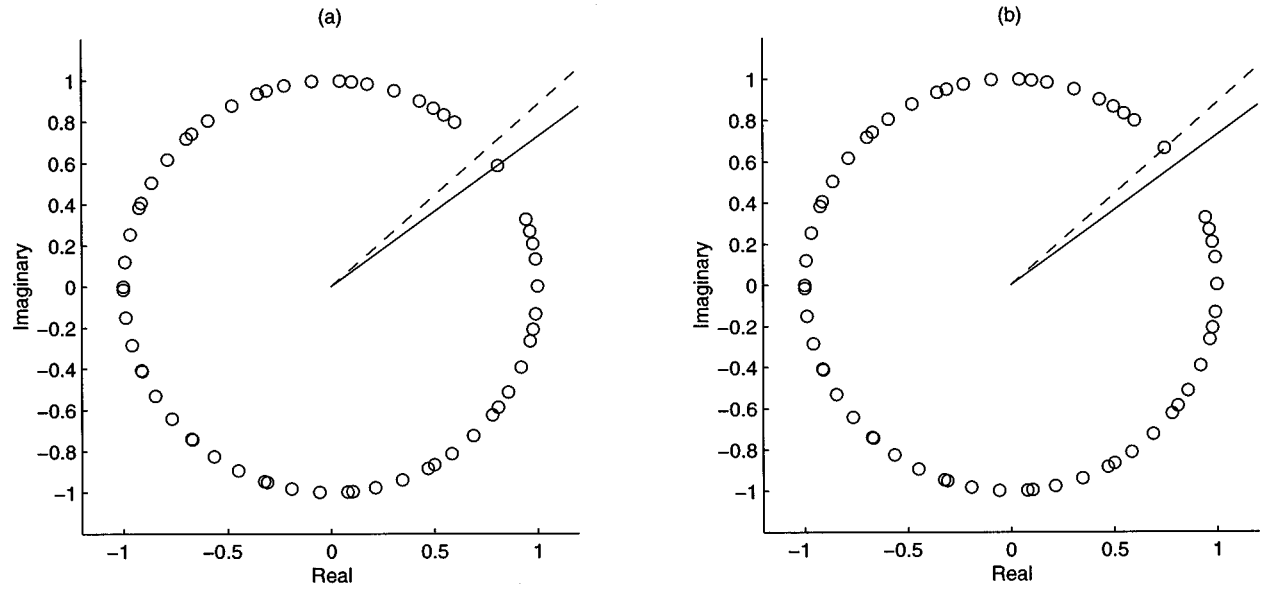

Fig. 6 Zeros of the simulated *A* line (a) before and (b) after ZAP. The solid line indicates the angular carrier frequency of the signal and the broken line indicates the angle that the ZAP zero subtends after ZAP.

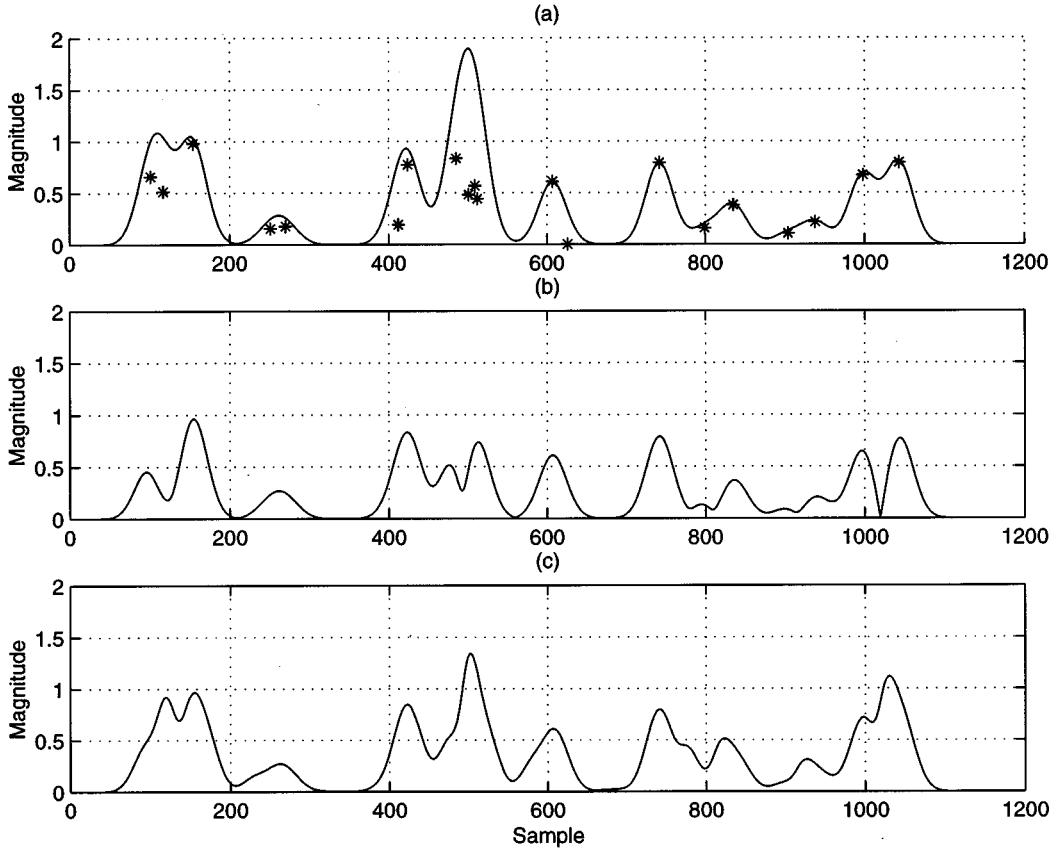

Fig. 7 A simulation of ZAP carried out for a sequence of point scatterers with random amplitudes and spacings. From top to bottom: (a) scatterers and profile of ideal backscatter signal, (b) simulated actual backscatter signal distorted by speckles, and (c) backscatter signal after application of ZAP.

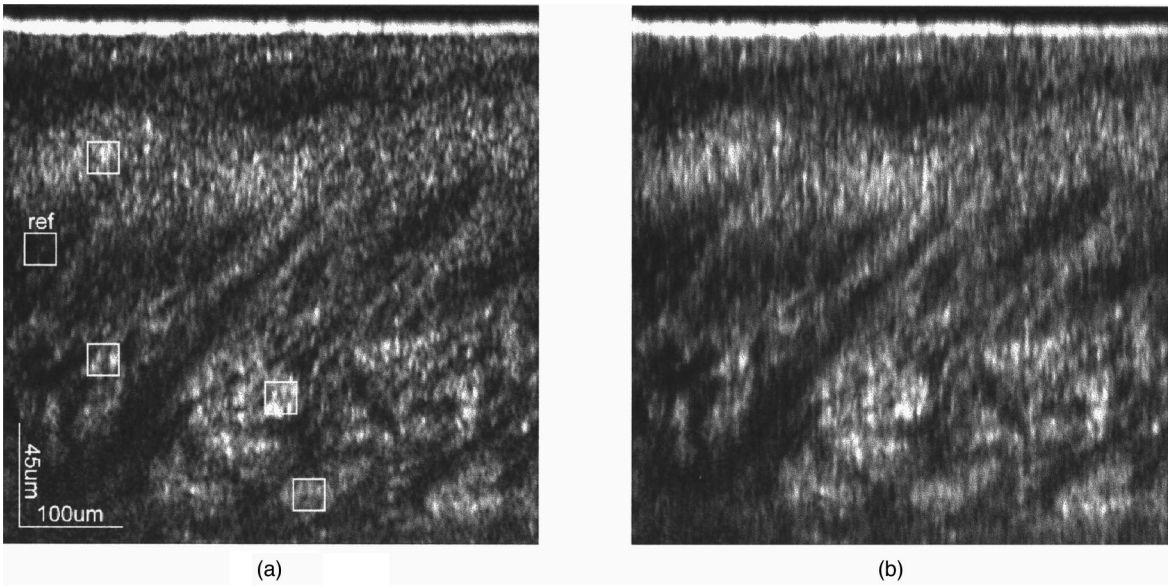

Fig. 8 OCT images of skin tissue at the back of the fifth finger before and after ZAP processing. The square labeled ''ref'' is the location of the reference window, while the others are the target windows used in the CNR calculations. All windows have dimensions of 32×32 pixels. (a) Image formed from the incoherent sum from four channels before ZAP. (b) Image formed from the incoherent sum of signals from each of the channels after ZAP.

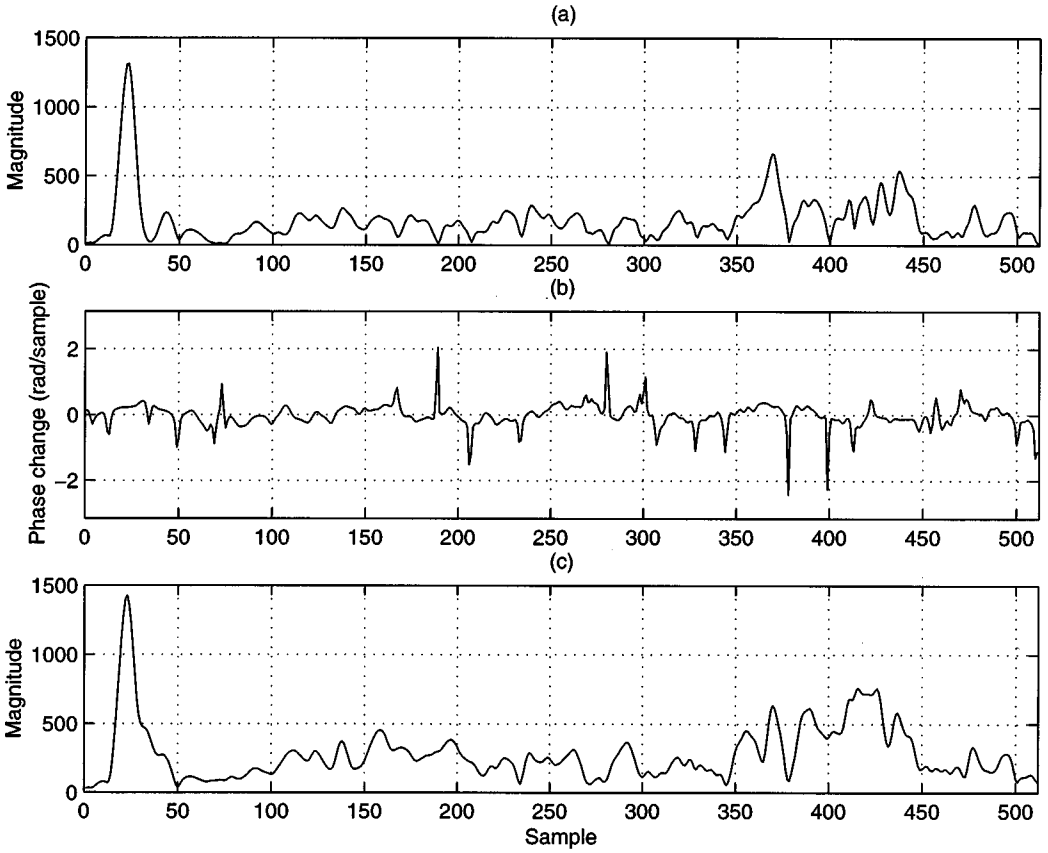

Fig. 9 Comparison of *A* lines from an OCT image of a channel (a) before and (b) after applying ZAP. (c) The phase changes of the original complex *A* line in which spikes indicate the occurrence of speckles.

reference windows (32×32 pixels) were placed in homogeneously speckled regions in the image and target areas of the same size were placed on recognizable features. The white square labeled ''ref'' in Figure 8(a) is the reference window and the others shown are the target windows. Table 1 gives the measured SNRs and CNRs of each of the four detector channels and their incoherent sums before and after ZAP. The CNRs were calculated by averaging the CNRs of the four targets.

After application of ZAP, both the SNR and CNR calculated from the individual and combined channels increased. Although the SNR increased substantially (by approximately 20% for each channel), the increase in CNR was generally much smaller, however, perhaps because blurring increased the mean level of the background intensity in the dark regions. Nonetheless, the results are consistent with the expectation that ZAP reduces speckle noise. Notice that the SNRs and CNRs for the sums of the channels are larger than those of the individual channels, as expected from the results of an earlier study.[14]

5 SUMMARY AND CONCLUSIONS

This study explored techniques for measurement and processing of OCT signals in the complex domain. Sampling and quadrature demodulation of the OCT signal with a laser clock were shown to be

Table 1 SNRs and CNRs of images before and after application of ZAP.

	Channel 1	Channel 2	Channel 3	Channel 4	Sum of four channels
SNR before ZAP	1.37	1.46	1.43	1.36	1.86
SNR after ZAP	1.68	1.75	1.75	1.63	2.22
CNR before ZAP	1.04	0.95	1.09	1.01	1.53
CNR after ZAP	1.32	1.18	1.35	1.30	1.97

essential for obtaining stable phase measurements. The laser reference removes the axial distortion and center frequency shifts of OCT signals sampled in the conventional asynchronous manner.

Our results suggest that the demodulated complex signals contain phase information related to the occurrence of destructive interference. Destructive interference occurs at positions along an A line at which the signal phase is large and abrupt. Large phase fluctuations may be a useful indicator of speckle. Simulations show that the zero-adjustment procedure (ZAP) provides an effective means of correcting speckle that results from near-simultaneous backscattering from nearby particles or clusters of particles. Operating in the z domain, ZAP associates speckle with the appearance of zeros at locations in the complex plane close to the angular carrier frequency. ZAP reconstruction is carried out by rotating the ZAP zeros away from the carrier frequency.

Application of ZAP to OCT images of skin tissue yielded promising results in preliminary experiments. The heavily speckled regions of the images appear smoother and the measured SNR of the images improved. However, the improvement appears to have been achieved at the expense of image blurring. As presently implemented, ZAP has a number of deficiencies. Although convenient, the thresholding and correction procedure on which ZAP is based have not yet been optimized in a general sense and do not react adaptively to fill in speckles with the proper amount of energy. It should be possible to improve the present ZAP algorithm by replacing the speckle detection procedure with an adaptive one that adjusts according to the spatial correlation of the phases of OCT signals measured with a multielement detector. Furthermore, combining ZAP with frequency-diversity methods[24] deserves investigation.

APPENDIX: MATHEMATICAL ANALYSIS OF ZAP FOR TWO SCATTERERS

A.1 DETECTION OF SPECKLES

The complex signal $y(n)$ is obtained by convolving the scatterer function $s(n)$ with the PSF $h(n)$ centered on a carrier with period R where R is an even integer greater than 2. The set of zeros of $Y(z)$ is the union of the sets of zeros of $H(z)$ and $S(z)$. The signals from scatterers of amplitudes α and β suffer from destructive interference when the scatterers are separated by an integer distance of $d=(N\pm 1/2)R$ for any integer N. For this case, the scatterer function is given by

$$s(n)=\begin{cases}\alpha, & n=0\\ \beta, & n=d=(N\pm\frac{1}{2})R\\ 0, & \text{otherwise},\end{cases} \tag{19}$$

which after z transformation, yields

$$S(z)=\alpha+\beta z^{-d}. \tag{20}$$

The zeros of this function in the z domain are located at

$$z=\left(\frac{\beta}{\alpha}\right)^{1/d} e^{j(2n-1)\pi/d}, \quad n=0,1,2,\ldots,d-1 \tag{21}$$

$$=\left(\frac{\beta}{\alpha}\right)^{1/d} e^{j2(2n-1)\pi/(2N\pm1)R},$$

$$n=0,1,2,\ldots,(N\pm\tfrac{1}{2})R-1. \tag{22}$$

There must exist an $n=(N+1/2)\pm 1/2$ such that

$$z=z_{\mathrm{ZAP}}=\left(\frac{\beta}{\alpha}\right)^{1/d} e^{j2\pi/R}. \tag{23}$$

The angular frequency of $y(n)$ is $\omega=2\pi/R$, which is the same as the frequency of the zero given by Eq. (23). This derivation shows that destructive interference must produce a zero (ZAP zero) at the signal angular frequency ω. As zeros of the PSF do not lie close to its angular carrier frequency, zeros near ω must be from the scatterer sequence. Therefore, the presence of a zero at or near ω indicates the presence of speckle.

A.2 CORRECTION OF DESTRUCTIVE INTERFERENCE EFFECTS

Express the z-transformed scatterer sequence $s(z)$ in terms of its zeros as in Eq. (20),

$$S(z)=\alpha+\beta z^{-d} \tag{A1}$$

$$=\alpha\prod_{k=0}^{d-1}\left[1-\frac{(\beta/\alpha)^{1/d}e^{-j(2k-1)\pi/d}}{z}\right]. \tag{A2}$$

Now rotate the positions of the ZAP zero in the z plane by increasing its phase by an angle δ. This is done by replacing $(\beta/\alpha)^{1/d}e^{j2\pi/R}$ by $(\beta/\alpha)^{1/d}e^{j2\pi/R}e^{j\delta}$ to obtain

$$S_{\mathrm{ZAP}}(z)=\frac{(\alpha+\beta z^{-d})\left[1-\dfrac{(\beta/\alpha)^{1/d}e^{j2\pi/R}e^{j\delta}}{z}\right]}{\left[1-\dfrac{(\beta/\alpha)^{1/d}e^{j2\pi/R}}{z}\right]}. \tag{A3}$$

$$=(\alpha+\beta z^{-d})\left[1+(1-e^{j\delta})\sum_{k=1}^{\infty}\frac{e^{j2k\pi/R}}{z^k}\right]. \tag{A4}$$

$S_{\mathrm{ZAP}}(z)$ cannot have order of z less than $-d$, so

$$S_{\mathrm{ZAP}}(z)=\alpha+\alpha(1-e^{j\delta})\times\sum_{k=1}^{d-1}\frac{e^{j2k\pi/R}}{z^{k}}+[\beta-\alpha(1-e^{j\delta})]\frac{1}{z^{d}}. \quad \text{(A5)}$$

For an OCT system with a sampled PSF $h(n)=g(n)e^{j2\pi n/\lambda}$, the corrected signal is then

$$Y_{\mathrm{ZAP}}(z)=H(z)S_{\mathrm{ZAP}}(z) \quad \text{(A6)}$$

$$=G(e^{-j2\pi/R}z)\left\{\alpha+\alpha(1-e^{j\delta})\times\sum_{k=1}^{d-1}\frac{e^{j2k\pi/R}}{z^{k}}+[\beta-\alpha(1-e^{j\delta})]\frac{1}{z^{d}}\right\}. \quad \text{(A7)}$$

Letting z be $e^{j2\pi/R}z$, we obtain

$$Y_{\mathrm{ZAP}}(e^{j2\pi/R}z)=G(z)\left\{\alpha+\alpha(1-e^{j\delta})\times\sum_{k=1}^{d-1}\frac{1}{z^{k}}+[\alpha(1-e^{j\delta})-\beta]\frac{1}{z^{d}}\right\}. \quad \text{(A8)}$$

After transforming this signal back to the spatial domain, we find

$$y_{\mathrm{ZAP}}(n)e^{-j2n\pi/R}=g(n)\otimes s_{\mathrm{ZAP}}(n), \quad \text{(A9)}$$

$$y_{\mathrm{ZAP}}(n)=\left\{\alpha g(n)+\alpha(1-e^{j\delta})\times\sum_{k=1}^{d-1}g(n-k)+[\alpha(1-e^{j\delta})-\beta]\times g(n-d)\right\}e^{j2n\pi/R}. \quad \text{(A10)}$$

The uncorrected speckled backscatter signal is given by Eq. (12), rewritten here as

$$y_{\mathrm{SPK}}(n)=[\alpha g(n)-\beta g(n-d)]e^{j2n\pi/R}, \quad \text{(A11)}$$

where $g(n)$ is related to $h(n)$ by Eq. (2). A comparison of this equation with Eq. (A10) reveals that ZAP adds a series of small complex numbers with amplitude $\alpha(1-e^{j\delta})$ at positions in the sequence between those of the original scatterers. Thus, when the ZAP-corrected sequence is convolved with $g(n)$ as in Eq. (A10), it fills up the destructively interfered region and reduces the distortion of the envelope caused by speckle.

REFERENCES

1. D. Huang, E. A. Swanson, C. P. Lin, J. S. Schuman, W. G. Stinson, W. Chang, M. R. Hee, T. Flotte, K. Gregory, C. A. Puliafito, and J. G. Fujimoto, "Optical coherence tomography," *Science* **254**, 1178–1181 (1991).
2. J. M. Schmitt, A. Knüttel, M. Yadlowsky, and R. F. Bonner, "Optical-coherence tomography of a dense tissue: Statistics of attenuation and backscattering," *Phys. Med. Biol.* **39**, 1705–1720 (1994).
3. J. A. Izatt, M. R. Hee, G. M. Owen, E. A. Swanson, and J. G. Fujimoto, "Optical coherence microscopy in scattering media," *Opt. Lett.* **19**, 590–592 (1994).
4. J. A. Izatt, M. D. Kulkarni, K. Kobayashi, M. V. Sivak, J. K. Barton, and A. J. Welch, "Optical coherence tomography for biodiagnostics," *Opt. Photonics News* **8**, 41–65 (1997).
5. D. A. Benaron, W. F. Cheong, and D. K. Stevenson, "Tissue optics," *Science* **276**, 2002–2003 (1997).
6. Y. Pan, E. Lankenau, J. Welzel, R. Birngruber, and R. Engelhardt, "Optical coherence-gated imaging of biological tissues," *IEEE J. Sel. Top. Quantum Electron.* **2**, 1029–1034 (1996).
7. T. Hellmuth, "Contrast and resolution in optical coherence tomography," *Proc. SPIE* **2926**, 228–237 (1996).
8. C. B. Burckhardt, "Speckle in ultrasound *B*-mode scans," *IEEE Trans. Sonics Ultrason.* **SU-25**, 1–6 (1978).
9. J. G. Abbott and F. L. Thurstone, "Acoustic speckle: theory and experimental analysis," *Ultrason. Imaging* **1**, 303–324 (1979).
10. L. M. Novak and M. C. Burl, "Optimal speckle reduction in polarimetric SAR imagery," *IEEE Trans. Aerosp. Electron. Syst.* **26**(2), 293–305 (1990).
11. D. A. Zimnyakov, V. V. Tuchin, and S. R. Utts, "A study of statistical properties of partially developed speckle fields as applied to the diagnostics of structural changes in human skin," *Opt. Spectrosc.* **76**, 838–844 (1994).
12. F. Forsberg, A. J. Healey, S. Leeman, and J. A. Jensen, "Assessment of hybrid speckle reduction algorithms," *Phys. Med. Biol.* **36**, 1539–1549 (1991).
13. *Laser Speckle and Related Phenomena*, J. C. Dainty, Ed., 2nd ed., Springer-Verlag, New York (1984).
14. J. M. Schmitt, "Array detection for speckle reduction in optical coherence microscopy," *Phys. Med. Biol.* **42**, 1427–1439 (1997).
15. B. Bouma, G. J. Tearney, S. A. Boppart, M. R. Hee, M. E. Brezinski, and J. G. Fujimoto, "High-resolution optical coherence tomographic imaging using a mode-locked Ti:Al_2O_3 laser source," *Opt. Lett.* **20**, 1486–1488 (1995).
16. J. M. Schmitt, S. L. Lee, and K. M. Yung, "An optical coherence microscope with enhanced resolving power," *Opt. Commun.* **142**, 203–207 (1997).
17. S. H. Xiang, L. Zhou, and J. M. Schmitt, "Speckle noise reduction for optical coherence tomography," *Proc. SPIE* **3196**, 79–88 (1997).
18. Z. P. Chen, T. E. Milner, S. Srinivas, X. J. Wang, A. Malekafzali, M. J. C. van Gemert, and J. S. Nelson, "Noninvasive imaging of *in vivo* blood flow velocity using optical Doppler tomography," *Opt. Lett.* **22**, 1–3 (1997).
19. J. A. Izatt and M. D. Kulkarni, "Doppler flow imaging using optical coherence tomography," presented at *OSA Conference on Lasers and Electro-Optics* (CLEO'96), Anaheim, CA, 1996, postdeadline paper No. CPD3-1.
20. A. J. Healey, F. Forsberg, and S. Leeman, "Processing techniques for speckle reduction in medical ultrasound images," *IEE Colloquium on "Image Processing in Medicine,"* No. 084 (1991).
21. A. J. Healey, S. Leeman, and F. Forsberg, "Turning off speckle," *Acoust. Imaging* **19**, 433–437 (1991).
22. J. W. Goodman, *Statistical Optics*, pp. 164–169, Wiley, New York (1985).
23. A. V. Oppenheim and R. W. Schafer, *Discrete-Time Signal Processing*, pp. 149–190, Prentice-Hall, Englewood Cliffs, NJ (1989).
24. H. E. Melton and P. A. Magnin, "*A*-mode speckle reduction with compound frequencies and compound bandwidths," *Ultrason. Imaging* **6**, 159–173 (1984).